Development and Precision Characterisation Of Broadband Anti-reflection-coated mm-wave Components

Matthew Lyons[a], Peter Hargrave[a], Ian Veenendaal[a], Rashmi Sudiwala[a], Carole Tucker[a], Ian Walker[a], Lottie Braithwaite[a], Berend Winter[b], Giorgio Savini[b], Alexey Shitvov[b], Jin Zhang [c], Jon E. Gudmundsson[d,e], and Giampaolo Pisano[f]

[a]Cardiff University, Queen's Buildings, The Parade, Cardiff, United Kingdom
[b]University College London, Physics Building, Gower St, London, United Kingdom
[c]Anglea Ruskin University, East Rd, Cambridge, United Kingdom
[d]University of Iceland, Science Institute, 107 Reykjavik, Iceland
[e]Stockholm University, The Oskar Klein Centre, Department of Physics, AlbaNova, SE-10691 Stockholm, Sweden
[e]Sapienza University of Rome, Piazzale Aldo Moro, 5, 00185 Roma RM, Italy

ABSTRACT

Future optical systems in the sub-mm range require low loss, low reflectance and broadband optics. Presented here is the development process for a hot press technique for making broadband multi-layer anti-reflection coatings for plastic lenses and optical components. The elevated temperatures used in this method induce a change in index and mechanical deformation in the substrate material due to polymer chain rearrangements. To avoid this, these components are annealed before they are machined to their intended form and prior to the application of any coating. Study of precise dimensional and refractive index changes between 115-130°C across repeated annealing cycles shows that ultra-high molecular weight polyethylene (UHMWPE) requires 3-4 annealing cycles above 125°C before stabilisation. We then present 3 and 5 layer test coating recipes for 90-225GHz with comparison between experimental measurements and theory. Preliminary results show good agreement. In this study, the methods presented are kept generic for any sub-mm band focusing broadly on 60-600GHz; however future work will apply what is achieved for future CMB experiments.

Keywords: axial refractive systems, optics, multi-layer coating, polymer lenses, sub-mm

1. INTRODUCTION

High throughput, diffraction-limited optical components are critical for state-of-the-art astronomy. This paper presents developments in the use of plastic optics and multi-layer anti-reflection (AR) coatings for this purpose. UHMW-PE plastic is ideal because of its low loss and moderately high refractive index which is constant in the microwave range.[1] Polyethylene is a common choice for lens material in sub-mm astronomy, for example: CLASS, EBEX, and BICEP/Keck Array.[2–4] Alternative materials for sub-mm optics include: silicon (e.g. ACTpol)[5] or alumina (e.g. Simons Array/POLARBEAR-2).[6] However, material availability, simpler procurement, cost, and end-of-life disposal are all concerns that are benefited by use of plastics optics.

The sub-mm reflectance for an untreated UHMW-PE test puck is $\sim 10\%$ highlighting the importance of an effective AR coating. Low reflectance is critical for reducing unwanted optical effects such as stray light, polarisation, and maximising the incident light upon the focal plane for detection. AR coatings typically have one or more dielectric layers stacked over the optical component with the intention of causing destructive interference between the outermost layer interface and subsequent layers. It follows that the thickness of the coating layer must be equal to one quarter of the desired target wavelength for destructive interference to occur. For broadband

Further author information: (Send correspondence to M.L.)
M.L.: E-mail: LyonsM4@cardiff.ac.uk
P.H.: E-mail: HargravePC@cardiff.ac.uk

Space Telescopes and Instrumentation 2024: Optical, Infrared, and Millimeter Wave, edited by Laura E. Coyle, Shuji Matsuura, Marshall D. Perrin, Proc. of SPIE Vol. 13092, 1309276 · © 2024 SPIE · 0277-786X · doi: 10.1117/12.3018886

low reflectance, multiple coating layers can be stacked. The refractive index of the coating layer n_l is determined by the geometric mean of the refractive indices of the media: $n_l = \sqrt{n_1 \cdot n_2}$. Vacuum: $n_1 = 1$ and UHMW-PE: $n_2 = \sim 1.526$. (Section 3.2) Due to the small thickness and low loss of possible coating materials, loss due to coating material is negligible. Meta-material sub-wavelength structures are a popular alternative to multi-layer coatings.[2] They work by machining a large number of repeated structures onto the surface of a substrate. These can be pyramids, stepped pyramids, repeating blocks, cones, or drilled bevels.[7,8] Dielectric properties can be manipulated in this way because these structures are smaller than the observation wavelength. However the fabrication of such structures requires a specialist multi-axis dicing saw system or CNC machines[2,9,10] .

This paper presents a hot-pressing technique for multi-layer AR coating which uses less specialist equipment and will build on a previous study that highlighted the importance of addressing thermal deformation.[11] Secondly, induced dimensional changes in the plastic substrate from this technique are also investigated and minimised with a proposed annealing cycle. Thirdly, multi-layer coating solutions are modelled and then experimentally verified.

2. EXPERIMENTAL DETAIL AND DATA COLLECTION

2.1 Annealing Cycles

Thermal deformation during the coating process presents the biggest challenge to the hot press method because the precise geometry of the optical component is critical to its ability to focus light. This study aimed to determine the number of annealing cycles required to stop heat-induced deformation in lens material due to rearrangements of polymer chains. To achieve this: test pucks with $\sim 10mm$ thickness and $\sim 70mm$ diameter were purchased from Ensinger Ltd. The pucks were prepared by precisely measuring diameter, thickness, and flatness (Section 2.3). Three pairs of pucks were then brought up to three set point temperatures respectively between $120 - 135°C$ respectively. To ensure accurate temperature measurement, a separate puck was prepared with a PT100 temperature sensor inserted into the puck such that the temperature from the centre of the puck could be recorded. It was assumed that this represents the temperature of the accompanying pucks in each cycle because the sensor was encased within the UHMW-PE. To ensure isothermal conditions in the puck, the oven was allowed to heat up to a stable temperature and left to sit for 7-8 hours. Since the efficiency of the oven would not allow the entire interior to be heated evenly to the intended set point, a further set of PT100 sensors were used to track temperature gradients within the oven.

A test range of $120 - 135°C$ was selected as the component needs to be hot enough for the glue to activate but not so hot that substrate melts. $120°C$ is above the melting point of the LDPE glue layers and $140°C$ is the melting point of UHMW-PE.[12,13] After the heating cycle is complete the oven is switched off and the pucks are allowed to cool unaided with an exponential drop off back to the ambient temperature of the lab. Note that in practice the oven used here had a $\sim 4°C$ discrepancy between commanded set-point and actual temperature of the sample. In practice, a $120°C$ set point resulted in the puck achieving $\sim 116°C$ for example.

A dimension change occurs in the pucks because the extrusion process used to produce stock material tends to force molecular chains into a common orientation aligned with direction of flow. The elevated temperatures allow the bonds between molecular chains to loosen and relax back into an unaligned orientation. This issue is mitigated by letting the plastic reach its relaxed state before forming it into a lens and coating it, hence the need for a refined annealing process.[14]

2.2 Transmission Measurements

The measurements of transmission in the UHMW-PE test pucks were performed using continuous-wave terahertz (cw-THz) spectroscopy. Optical heterodyning of two incident electromagnetic (EM) waves of adjacent frequencies within an InGaAs photomixer produces a new wave at the beat frequency of the two waves. This signal is output as an EM wave by a log spiral antenna. In this case, 2 NIR lasers interfere to produce EM waves up to 1.2 THz. In practice this limit is set at $\sim$ 1THz as maintaining coherence of the distributed feedback *(DFB)* lasers at higher frequencies is difficult as they are temperature controlled. The receiver is similarly configured with with a log spiral antenna InGaAs photomixer coupled to a silicon lens. It is illuminated by the signal passing the test sample and one of the initial laser signals is used as reference for lock-in detection. The resulting photocurrent

is proportional to the energy of the signal amplitude through the material. Transmission can then be recovered by comparison of a noise background and signal in the material.[10,15,16]

2.3 Metrology

Precise record of any changes in the dimensions of the pucks post-annealing is essential. For this investigation and due to size constraints, a digital micrometer and caliper were used for thickness and diameter measurements respectively. Multiple diameter measurements were recorded at 3 positions along the puck; bottom, middle and top. This was intended to capture any tapering or inhomogenous deformation. It was assumed that any tapering would be small enough for volume to be calculated as a cylinder with the average of diameters across the 3 possible heights. Similarly the digital micrometer was used to record thickness along the circumference edge and range of positions closer to the centre to observe any variable change in thickness. For analysis involving thickness measurements, (Section 3.2), the average of the thickness within 20mm of the centre of the puck were used as $> 90\%$ beam falls within that radius.

3. RESULTS AND ANALYSIS

3.1 Examining Shape Deformation

Tracking the diameter and thickness changes for a group of sample pucks between $115 - 130°C$ shows that four annealing cycles are required for shape change to fall to below 0.1% for all pucks. Figure 1 shows a decrease in diameter and increase in thickness. This is caused by the relaxation of molecules in the opposite direction in which the plastic was compressed during extrusion.[14] Three annealing cycles are required for stabilisation of diameter and thickness. The condition for "stable" used here is a $< 0.1\%$ change in diameter and thickness between cycles. In terms of temperature selection, the hotter annealing cycles are no quicker at achieving stabilisation than the colder cycles, diameter and thickness consistently require three cycles to reach a $< 0.1\%$ change. A stricter stabilisation threshold lower than $< 0.1\%$ would shows that the $\sim 116°C$ is less stable for the same number of cycles than $\sim 121°C$ or $\sim 131°C$. This fact coupled with the need to melt the LDPE glue layers and not the UHMW-PE material will inform further studies to focus on annealing set points $125°C > T > 135°C$.

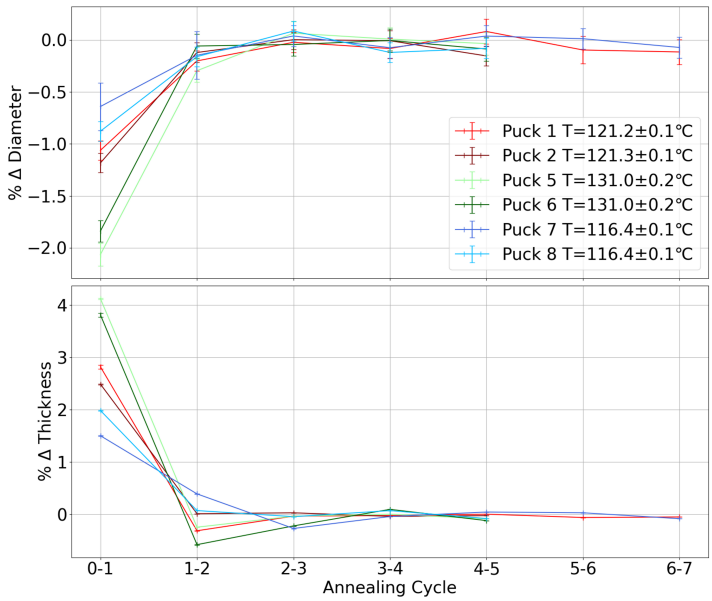

Figure 1: Metrology percentage change between cycles. TOP: The % diameter change and BOTTOM : % thickness stabilises after 3 cycles within 115-130°C range.

3.2 Recovering Refractive Index

Photocurrent data (Section 2.2) can be used to extract refractive index: the Fourier transform of the photocurrent signal expresses the signal as a function of the cavity length. Performing this operation for both sample and background measurements, then finding the most prominent peak feature's cavity position, and finally subtracting them gives the path difference. This result is invariant of signal strength so long as you can identify the same feature between the spectra. Uncertainty only propagates from frequency resolution of the scanning equipment. Path difference, δ, and sample thickness, T, relate to give refractive index, n:

$$n = \frac{2\delta}{T} + 1 \tag{1}$$

3.3 Evolution of Volume and Refractive Index

Recovering volume and refractive index as a function of annealing cycle shows a linear decrease and increase respectively. R-square tests indicate good fit with all fits shown on figure 2 having values $0.6 - 1$. Given that mass remains constant,[17] the density is increasing; this indicates a correlation between substrate density and refractive index.

For similar temperatures, the linear fit gradients agree; this implies that for hotter temperatures, we observe steeper gradients and vice versa. This can be seen for both volume and refractive index plots in figure 2. The measurement errors (section 2.3) for diameter were one order of magnitude worse than for thickness. So within the volume calculation, this diameter error propagates with twice the weighting due to squaring in the calculation hence the larger error margin. Plotting gradient as a function of annealing temperature allows us to begin to interpolate expected metrology change over the range used in this investigation. For a full fit to be performed, more repeated measurements are required. The evolution of volume is observed on figure 2 because small changes in thickness and diameter are amplified when multiplied. Recall that the threshold for stabilisation used here is $\sim 0.1\%$; future studies may require stricter stabilisation conditions. For manufacture of optics components, this threshold should be set by the tolerance required to maintain lens geometry and its focus.

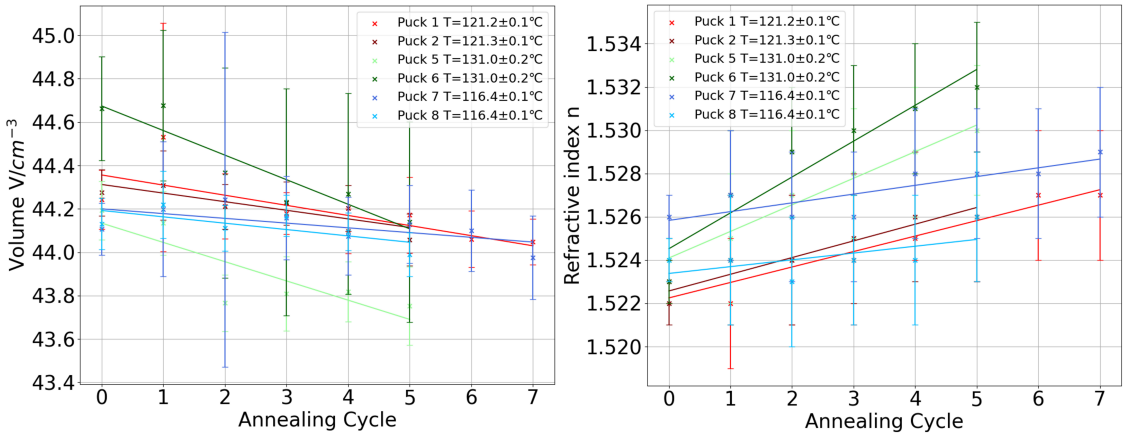

Figure 2: LEFT: Volume & RIGHT: Refractive Index Change with Cycle at 115-130°C. A linear decrease in volume & linear increase in refractive index between cycle can be seen. The change in volume implies an increasing density.

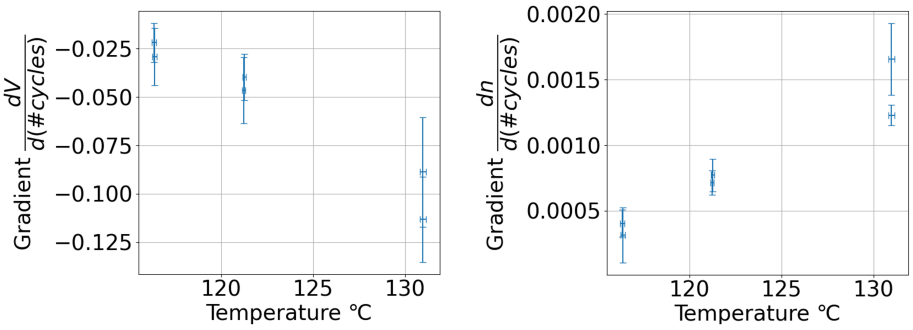

Figure 3: LEFT: Volume change and RIGHT: refractive index change per cycle vs annealing temperature. From this, the gradients at intermediate temperatures can be inferred, thus enabling a prediction of volume and refractive index change to be made.

4. MANUFACTURING AND TESTING MULTI-LAYER ARCS

To produce test samples, layers of coating material and an annealed UHMW-PE puck were mounted in a vacuum rig, they were then heated to a set point of 135 °C for 8 hours. The coating scheme used here involved interspersed layers of porous polytetrafluoroethylene (pPTFE) and cast polypropylene (CPP). Low-density polyethylene (LDPE) was used as a bonding layer between layers. The recipes for 2 test samples are shown in tables1 and 2.

Figures 4 and 5 show transmission results for the preliminary run of hot pressing for 3- and 5-layer AR coatings. The 3-layer AR coating matches the transfer matrix model (TMM) prediction with good accuracy. The low frequency noise and shorter peaks are likely due to the instrumentation and sampling constraints of the Fourier-transform spectrometer (FTS) used for measurement. The 5-layer transmission displays poorer agreement with the model, however the model likely requires refined thickness and refractive index measurements of the intermediate layers. For example, during the coating process the layers are compressed and so their thickness may change. These test pucks were also coated before annealing so will show shape deformation effects.

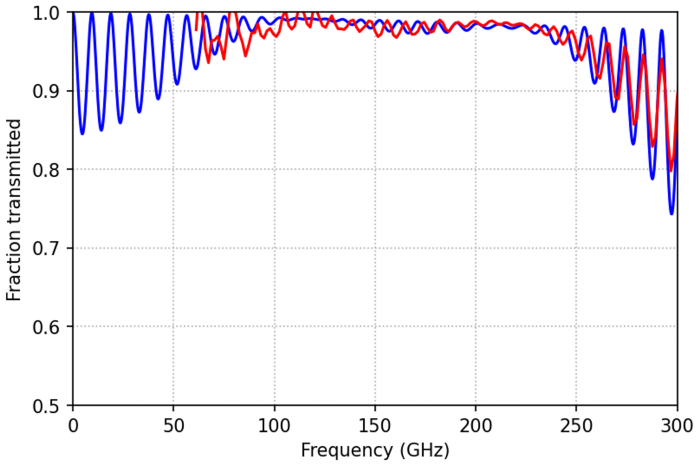

Figure 4: 3 Layer AR Coating showing agreement between the modelling and data collection. Red: FTS measurement. Blue: Prediction of transmission using TMM.

Layer	Material	Ref. Index	μm
1	**pPTFE**	**1.15**	**415**
	LDPE	1.5141	6
2	**CPP**	**1.51**	**110**
	LDPE	1.5141	6
3	**pPTFE**	**1.15**	**127**
	LDPE	1.5141	6
L	UHMWPE	1.527	10020
Symmetric on the reverse side			

Table 1: Recipe for 3 layer AR coating on a UHMW-PE puck using the hot press method.

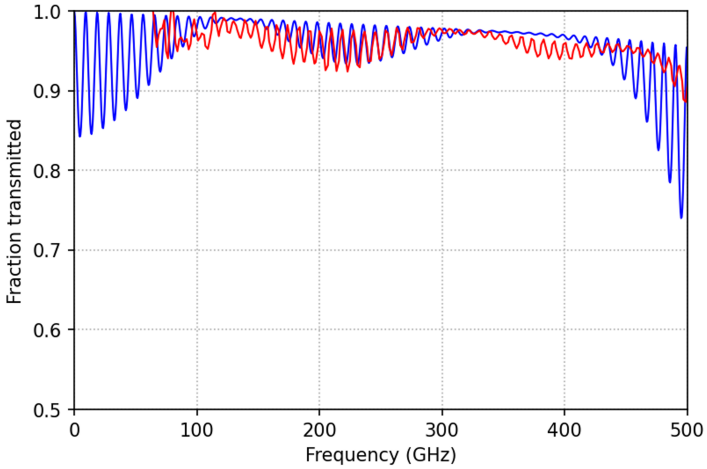

Figure 5: 5 Layer AR Coating showing some agreement between the modelling and data collection. Red: FTS measurement. Blue: Prediction of transmission using TMM.

Layer	Material	Ref. Index	μm
1	**pPTFE**	**1.15**	**250**
	LDPE	1.5141	6
2	**CPP**	**1.51**	**57**
	LDPE	1.5141	6
3	**pPTFE**	**1.15**	**127**
	LDPE	1.5141	6
4	**CPP**	**1.51**	**67**
	LDPE	1.5141	6
5	**pPTFE**	**1.15**	**55**
L	UHMWPE	1.527	10020
Symmetric on the reverse side			

Table 2: Recipe for 5 layer AR coating on a UHMW-PE puck using the hot press method.

5. MODELLING IDEAL MULTI-LAYER ARC RECIPES

The TMM code can be adapted to create an optimisation program to maximise transmission. The program iterates through a desired range of possible thicknesses at a set interval, calculates the average transmission for a specific frequency band. The best average transmission and the associated recipe is then returned. The program is run for 3 and 5 layers depending on time and computer processing power. The recipe conditions applied for this paper are as outlined in table 3. For illustrative purposes, figure 6 presents a possible 3 layer AR coating optimised for the LiteBIRD MFT band (89-225GHz).[18] Average in band transmission is 0.995. Note that this is only a representative proposed recipe; for this to be practical, the model would have to be re-run to iterate with layer thicknesses that are able to be procured. Here, coating layers are chosen between 50-500 microns in increments of 50 microns. Further study of refractive index and loss within the substrate material stock also requires full characterisation.

Layer	Material	Ref. Index	μm
1	**pPTFE**	**1.15**	**Free variable**
	LDPE	1.5141	6
2	**CPP**	**1.51**	**Free variable**
	LDPE	1.5141	6
3	**pPTFE**	**1.15**	**Free variable**
	LDPE	1.5141	6
4	**CPP**	**1.51**	**Free variable**
	LDPE	1.5141	6
5	**pPTFE**	**1.15**	**Free variable**
L	UHMWPE	1.524	10000
Symmetric on the reverse side			

Table 3: Recipe for which the code optimises. Shown here is the 5 layer permutation, the 3 layer verison omits one layer of CPP and pPTFE with their LDPE bonding layers. CPP and pPTFE have variable thickness: $50 - 500\mu m$ iterating over 10 steps of $50\mu m$ to find an optimised recipe with the most transmission.

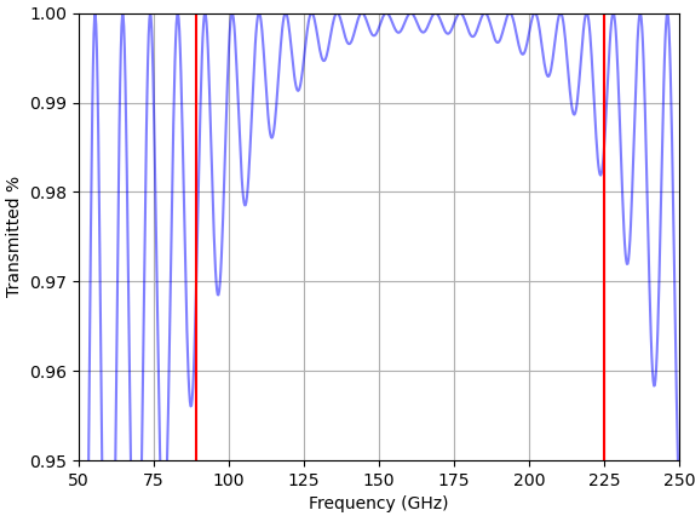

Figure 6: Proposed model for 3 layer AR coating optimised for LiteBIRD MFT 89-225GHz (red lines). Average transmission in-band: 0.995.

Layer	Material	Ref. Index	μm
1	**pPTFE**	**1.15**	**400**
	LDPE	1.5141	6
2	**CPP**	**1.51**	**150**
	LDPE	1.5141	6
3	**pPTFE**	**1.15**	**50**
	LDPE	1.5141	6
L	UHMWPE	1.524	10000
Symmetric on the reverse side			

Table 4: Optimised recipe for 3 layer AR coating for LiteBIRD MFT 89-22GHz.

6. CONCLUSION AND APPLICATION TO FUTURE MISSIONS

With regard to the development of low loss, low reflectance and broadband anti-reflection coatings: we reported on the development of an annealing cycle treatment for UHMW-PE to minimise thermal deformation. At least three cycles with a puck temperature between $125°C > T > 135°C$ are required to achieve this. We also presented the results from a first attempt at using a hot press method to coat sample test pucks. Results show good agreement for transmission between the transfer matrix method and experimental data. Finally, the TMM code has been used to present potential optimised coating recipes for further study and direct future sample AR coatings before full lens production.

The next stage of the study involves understanding the coefficient of thermal expansion (CTE) for the lens material. This will enable the lens to have correct shape during cold operation despite having been machined while warm. Similarly, the evolution of refractive index down to cold temperatures will also need to be well understood for telescope operation .

This report is broadly applicable to the entire field of sub-mm astronomy, but will specifically benefit very wide field, high throughput experiments with particular application to CMB studies.

ACKNOWLEDGMENTS

The transfer matrix method program used in creating the optimisation model for the anti reflection coating recipes was published by S.J. Byrnes.[19] Full credit for Python package "TMM" is given to them.

REFERENCES

[1] D'Alessandro, G., Paiella, A., Coppolecchia, A., Castellano, M. G., Colantoni, I., de Bernardis, P., Lamagna, L., and Masi, S., "Ultra high molecular weight polyethylene: Optical features at millimeter wavelengths," *Infrared Physics & Technology* **90**, 59–65 (May 2018).

[2] Essinger-Hileman, T., Ali, A., Amiri, M., Appel, J. W., Araujo, D., Bennett, C. L., Boone, F., Chan, M., Cho, H.-M., Chuss, D. T., Colazo, F., Crowe, E., Denis, K., Dünner, R., Eimer, J., Gothe, D., Halpern, M., Harrington, K., Hilton, G., Hinshaw, G. F., Huang, C., Irwin, K., Jones, G., Karakla, J., Kogut, A. J., Larson, D., Limon, M., Lowry, L., Marriage, T., Mehrle, N., Miller, A. D., Miller, N., Moseley, S. H., Novak, G., Reintsema, C., Rostem, K., Stevenson, T., Towner, D., U-Yen, K., Wagner, E., Watts, D., Wollack, E., Xu, Z., and Zeng, L., "CLASS: The Cosmology Large Angular Scale Surveyor," 91531I (July 2014). arXiv:1408.4788 [astro-ph].

[3] Collaboration, T. E., Aboobaker, A. M., Ade, P., Araujo, D., Aubin, F., Baccigalupi, C., Bao, C., Chapman, D., Didier, J., Dobbs, M., Geach, C., Grainger, W., Hanany, S., Helson, K., Hillbrand, S., Hubmayr, J., Jaffe, A., Johnson, B., Jones, T., Klein, J., Korotkov, A., Lee, A., Levinson, L., Limon, M., MacDermid, K., Matsumura, T., Miller, A. D., Milligan, M., Raach, K., Reichborn-Kjennerud, B., Sagiv, I., Savini, G., Spencer, L., Tucker, C., Tucker, G. S., Westbrook, B., Young, K., and Zilic, K., "The EBEX Balloon-borne Experiment—Optics, Receiver, and Polarimetry," *The Astrophysical Journal Supplement Series* **239**, 7 (Nov. 2018). Publisher: The American Astronomical Society.

[4] Ade, P. A. R., Ahmed, Z., Amiri, M., Barkats, D., Thakur, R. B., Bischoff, C. A., Beck, D., Bock, J. J., Boenish, H., Bullock, E., Buza, V., IV, J. R. C., Connors, J., Cornelison, J., Crumrine, M., Cukierman, A., Denison, E. V., Dierickx, M., Duband, L., Eiben, M., Fatigoni, S., Filippini, J. P., Fliescher, S., Goeckner-Wald, N., Goldfinger, D. C., Grayson, J., Grimes, P., Hall, G., Halal, G., Halpern, M., Hand, E., Harrison, S., Henderson, S., Hildebrandt, S. R., Hilton, G. C., Hubmayr, J., Hui, H., Irwin, K. D., Kang, J., Karkare, K. S., Karpel, E., Kefeli, S., Kernasovskiy, S. A., Kovac, J. M., Kuo, C. L., Lau, K., Leitch, E. M., Lennox, A., Megerian, K. G., Minutolo, L., Moncelsi, L., Nakato, Y., Namikawa, T., Nguyen, H. T., O'Brient, R., IV, R. W. O., Palladino, S., Prouve, T., Pryke, C., Racine, B., Reintsema, C. D., Richter, S., Schillaci, A., Schwarz, R., Schmitt, B. L., Sheehy, C. D., Soliman, A., Germaine, T. S., Steinbach, B., Sudiwala, R. V., Teply, G. P., Thompson, K. L., Tolan, J. E., Tucker, C., Turner, A. D., Umiltà, C., Vergès, C., Vieregg, A. G., Wandui, A., Weber, A. C., Wiebe, D. V., Willmert, J., Wong, C. L., Wu, W. L. K., Yang, H., Yoon, K. W., Young, E., Yu, C., Zeng, L., Zhang, C., Zhang, S., and Collaboration), B. K., "Bicep/Keck XV: The Bicep3 Cosmic Microwave Background Polarimeter and the First Three-year Data Set," *The Astrophysical Journal* **927**, 77 (Mar. 2022). Publisher: The American Astronomical Society.

[5] Thornton, R. J., Ade, P. A. R., Aiola, S., Angile, F. E., Amiri, M., Beall, J. A., Becker, D. T., Cho, H.-M., Choi, S. K., Corlies, P., Coughlin, K. P., Datta, R., Devlin, M. J., Dicker, S. R., Dunner, R., Fowler, J. W., Fox, A. E., Gallardo, P. A., Gao, J., Grace, E., Halpern, M., Hasselfield, M., Henderson, S. W., Hilton, G. C., Hincks, A. D., Ho, S. P., Hubmayr, J., Irwin, K. D., Klein, J., Koopman, B., Li, D., Louis, T., Lungu, M., Maurin, L., McMahon, J., Munson, C. D., Naess, S., Nati, F., Newburgh, L., Nibarger, J., Niemack, M. D., Niraula, P., Nolta, M. R., Page, L. A., Pappas, C. G., Schillaci, A., Schmitt, B. L., Sehgal, N., Sievers, J. L., Simon, S. M., Staggs, S. T., Tucker, C., Uehara, M., van Lanen, J., Ward, J. T., and Wollack, E. J., "The Atacama Cosmology Telescope: The polarization-sensitive ACTPol instrument," *The Astrophysical Journal Supplement Series* **227**, 21 (Dec. 2016). arXiv:1605.06569 [astro-ph].

[6] Suzuki, A., Ade, P., Akiba, Y., Aleman, C., Arnold, K., Baccigalupi, C., Barch, B., Barron, D., Bender, A., Boettger, D., Borrill, J., Chapman, S., Chinone, Y., Cukierman, A., Dobbs, M., Ducout, A., Dunner, R., Elleflot, T., Errard, J., Fabbian, G., Feeney, S., Feng, C., Fujino, T., Fuller, G., Gilbert, A., Goeckner-Wald, N., Groh, J., Haan, T. D., Hall, G., Halverson, N., Hamada, T., Hasegawa, M., Hattori, K., Hazumi, M., Hill, C., Holzapfel, W., Hori, Y., Howe, L., Inoue, Y., Irie, F., Jaehnig, G., Jaffe, A., Jeong, O., Katayama, N., Kaufman, J., Kazemzadeh, K., Keating, B., Kermish, Z., Keskitalo, R., Kisner, T., Kusaka, A., Jeune, M. L., Lee, A., Leon, D., Linder, E., Lowry, L., Matsuda, F., Matsumura, T., Miller, N., Mizukami, K., Montgomery, J., Navaroli, M., Nishino, H., Peloton, J., Poletti, D., Puglisi, G., Rebeiz, G., Raum, C., Reichardt, C., Richards, P., Ross, C., Rotermund, K., Segawa, Y., Sherwin, B., Shirley, I., Siritanasak, P., Stebor, N., Stompor, R., Suzuki, J., Tajima, O., Takada, S., Takakura, S., Takatori, S., Tikhomirov, A., Tomaru, T., Westbrook, B., Whitehorn, N., Yamashita, T., Zahn, A., and Zahn, O., "The Polarbear-2 and the Simons Array Experiments," *Journal of Low Temperature Physics* **184**, 805–810 (Aug. 2016). Publisher: Springer ADS Bibcode: 2016JLTP..184..805S.

[7] Golec, J. E., McMahon, J. J., Ali, A. M., Chesmore, G. E., Cooperrider, L., Dicker, S., Galitzki, N., Harrington, K., Jackson, R., Westbrook, B., Wollack, E. J., Xu, Z., and Zhu, N., "Design and Fabrication of Metamaterial Anti-Reflection Coatings for the Simons Observatory," in [*Advances in Optical and Mechanical Technologies for Telescopes and Instrumentation IV*], 199 (Dec. 2020). arXiv:2101.10298 [astro-ph].

[8] Tapia, V., Rodríguez, R., Reyes, N., Mena, F. P., Yagoubov, P., Cuttaia, F., and Bronfman, L., "Systematic study of the cross polarization introduced by broadband antireflection layers at microwave frequencies," *Applied Optics* **57**, 9223–9229 (Nov. 2018). Publisher: Optica Publishing Group.

[9] Datta, R., Munson, C. D., Niemack, M. D., McMahon, J. J., Britton, J., Wollack, E. J., Beall, J., Devlin, M. J., Fowler, J., Gallardo, P., Hubmayr, J., Irwin, K., Newburgh, L., Nibarger, J. P., Page, L., Qui-

jada, M. A., Schmitt, B. L., Staggs, S. T., Thornton, R., and Zhang, L., "Large-aperture wide-bandwidth antireflection-coated silicon lenses for millimeter wavelengths," *Applied Optics* **52**, 8747–8758 (Dec. 2013). Publisher: Optica Publishing Group.

[10] Golec, J. E., Sutariya, S., Jackson, R., Zimmerman, J., Dicker, S. R., Iuliano, J., McMahon, J., Puglisi, G., Tucker, C., and Wollack, E. J., "Simons Observatory: Broadband Metamaterial Anti-Reflection Cuttings for Large Aperture Alumina Optics," *Applied Optics* **61**, 8904 (Oct. 2022). arXiv:2208.02292 [astro-ph, physics:physics].

[11] Pisano, G., Ng, R., Zhu, C., Tucker, C., and Ade, P., "Multi-octave anti-reflection coating for polypropylene-based quasi-optical devices," in [*Millimeter, Submillimeter, and Far-Infrared Detectors and Instrumentation for Astronomy IX*], **10708**, 1138–1144, SPIE (July 2018).

[12] Prasad, A., "A quantitative analysis of low density polyethylene and linear low density polyethylene blends by differential scanning calorimetery and fourier transform infrared spectroscopy methods," *Polymer Engineering & Science* **38**(10), 1716–1728 (1998). _eprint: https://onlinelibrary.wiley.com/doi/pdf/10.1002/pen.10342.

[13] Wang, X. and Salovey, R., "Melting of ultrahigh molecular weight polyethylene," *Journal of applied polymer science.* **34** (Aug. 1987). Place: New York, Publisher: Wiley.

[14] Sambasvian, S., Fischer, D. A., Shen, M. C., Tesk, J. A., and Hsu, S. M., "Effects of Annealing on UHMWPE Molecular Orientation," *NIST* **51** (Jan. 2000). Last Modified: 2021-10-12T11:10-04:00 Publisher: S Sambasvian, Daniel A. Fischer, M C. Shen, John A. Tesk, Stephen M. Hsu.

[15] Deninger, A., "11 - State-of-the-art in terahertz continuous-wave photomixer systems," in [*Handbook of Terahertz Technology for Imaging, Sensing and Communications*], Saeedkia, D., ed., *Woodhead Publishing Series in Electronic and Optical Materials*, 327–373, Woodhead Publishing (Jan. 2013).

[16] "TeraScan 1550/TeraBeam 1550 Manual," (2019).

[17] Lamri, A., Shirinbayan, M., Pereira, M., Truffault, L., Fitoussi, J., Lamouri, S., Bakir, F., and Tcharkhtchi, A., "Effects of strain rate and temperature on the mechanical behavior of high-density polyethylene," *Journal of Applied Polymer Science* **137**(23), 48778 (2020). Publisher: Wiley.

[18] Collaboration, L., Allys, E., Arnold, K., Aumont, J., Aurlien, R., Azzoni, S., Baccigalupi, C., Banday, A. J., Banerji, R., Barreiro, R. B., Bartolo, N., Bautista, L., Beck, D., Beckman, S., Bersanelli, M., Boulanger, F., Brilenkov, M., Bucher, M., Calabrese, E., Campeti, P., Carones, A., Casas, F. J., Catalano, A., Chan, V., Cheung, K., Chinone, Y., Clark, S. E., Columbro, F., D'Alessandro, G., de Bernardis, P., de Haan, T., de la Hoz, E., De Petris, M., Della Torre, S., Diego-Palazuelos, P., Dobbs, M., Dotani, T., Duval, J. M., Elleflot, T., Eriksen, H. K., Errard, J., Essinger-Hileman, T., Finelli, F., Flauger, R., Franceschet, C., Fuskeland, U., Galloway, M., Ganga, K., Gerbino, M., Gervasi, M., Génova-Santos, R. T., Ghigna, T., Giardiello, S., Gjerløw, E., Grain, J., Grupp, F., Gruppuso, A., Gudmundsson, J. E., Halverson, N. W., Hargrave, P., Hasebe, T., Hasegawa, M., Hazumi, M., Henrot-Versillé, S., Hensley, B., Hergt, L. T., Herman, D., Hivon, E., Hlozek, R. A., Hornsby, A. L., Hoshino, Y., Hubmayr, J., Ichiki, K., Iida, T., Imada, H., Ishino, H., Jaehnig, G., Katayama, N., Kato, A., Keskitalo, R., Kisner, T., Kobayashi, Y., Kogut, A., Kohri, K., Komatsu, E., Komatsu, K., Konishi, K., Krachmalnicoff, N., Kuo, C. L., Lamagna, L., Lattanzi, M., Lee, A. T., Leloup, C., Levrier, F., Linder, E., Luzzi, G., Macias-Perez, J., Maciaszek, T., Maffei, B., Maino, D., Mandelli, S., Martínez-González, E., Masi, S., Massa, M., Matarrese, S., Matsuda, F. T., Matsumura, T., Mele, L., Migliaccio, M., Minami, Y., Moggi, A., Montgomery, J., Montier, L., Morgante, G., Mot, B., Nagano, Y., Nagasaki, T., Nagata, R., Nakano, R., Namikawa, T., Nati, F., Natoli, P., Nerval, S., Noviello, F., Odagiri, K., Oguri, S., Ohsaki, H., Pagano, L., Paiella, A., Paoletti, D., Passerini, A., Patanchon, G., Piacentini, F., Piat, M., Pisano, G., Polenta, G., Poletti, D., Prouvé, T., Puglisi, G., Rambaud, D., Raum, C., Realini, S., Reinecke, M., Remazeilles, M., Ritacco, A., Roudil, G., Rubino-Martin, J. A., Russell, M., Sakurai, H., Sakurai, Y., Sasaki, M., Scott, D., Sekimoto, Y., Shinozaki, K., Shiraishi, M., Shirron, P., Signorelli, G., Spinella, F., Stever, S., Stompor, R., Sugiyama, S., Sullivan, R. M., Suzuki, A., Svalheim, T. L., Switzer, E., Takaku, R., Takakura, H., Takase, Y., Tartari, A., Terao, Y., Thermeau, J., Thommesen, H., Thompson, K. L., Tomasi, M., Tominaga, M., Tristram, M., Tsuji, M., Tsujimoto, M., Vacher, L., Vielva, P., Vittorio, N., Wang, W., Watanuki, K., Wehus, I. K., Weller, J., Westbrook, B., Wilms, J., Winter, B., Wollack, E. J., Yumoto, J., and Zannoni, M., "Probing Cosmic Inflation with the LiteBIRD Cosmic Microwave

Background Polarization Survey," *Progress of Theoretical and Experimental Physics* **2023**, 042F01 (Apr. 2023). arXiv:2202.02773 [astro-ph].

[19] Byrnes, S. J., "Multilayer optical calculations," (Dec. 2020). arXiv:1603.02720 [physics].